Extended optical model analyses of elastic scattering and fusion cross section data for the ^{7}Li + ^{208}Pb system at near-Coulomb-barrier energies using a folding potential

W. Y. So and T. Udagawa
Department of Physics, University of Texas, Austin, Texas 78712, USA

K. S. Kim
Department of Liberal Arts and Science, Hankuk Aviation University, Koyang 412-791, Korea

S. W. Hong and B. T. Kim
Department of Physics and Institute of Basic Science, Sungkyunkwan University, Suwon 440-746, Korea
(Received 1 June 2007; published 29 August 2007)

Simultaneous χ^2 analyses previously made for elastic scattering and fusion cross section data for the ^{6}Li + ^{208}Pb system are extended to the ^{7}Li + ^{208}Pb system at near-Coulomb-barrier energies based on the extended optical model approach, in which the polarization potential is decomposed into direct reaction (DR) and fusion parts. Use is made of the double folding potential as a bare potential. It is found that the experimental elastic scattering and fusion data are well reproduced without introducing any normalization factor for the double folding potential and that both the DR and fusion parts of the polarization potential determined from the χ^2 analyses satisfy separately the dispersion relation. Further, we find that the real part of the fusion portion of the polarization potential is attractive while that of the DR part is repulsive except at energies far below the Coulomb barrier energy. A comparison is made of the present results with those obtained from the coupled discretized continuum channels calculations and a previous study based on the conventional optical model with a double folding potential. We also compare the present results for the ^{7}Li + ^{208}Pb system with the analysis previously made for the ^{6}Li + ^{208}Pb system.

DOI: 10.1103/PhysRevC.76.024613 PACS number(s): 24.10.Ht, 25.70.Bc, 25.70.Jj

I. INTRODUCTION

It has been a long standing problem that one is forced to reduce the strength of the folding potential by a factor $N = 0.5 \sim 0.6$ to reproduce the elastic scattering data [1,2] for loosely bound projectiles such as ^{6}Li and ^{9}Be within the optical model approach with a folding potential. This problem has been ascribed to the strong breakup character of the projectiles; studies have been made of the effects of the breakup on the elastic scattering, based on the coupled discretized continuum channels (CDCC) method [3,4]. These studies were very successful in reproducing the elastic scattering data without introducing any arbitrary normalization factor and furthermore in understanding the physical origin of the factor $N = 0.5 \sim 0.6$ needed to be introduced in one-channel optical model calculations. The authors of Refs. [3] and [4] projected their coupled-channels equations to a single elastic channel equation and deduced the polarization potential arising from the coupling with the breakup channels. The resultant real part of the polarization potential was then found to be repulsive at the surface region around the strong absorption radius, R_{sa}. This shows that the reduction of the folding potential by a factor of $N = 0.5 \sim 0.6$ effectively takes into account the effects of this repulsive coupling with the breakup channels.

In our recent study [5], we explored this problem for the ^{6}Li + ^{208}Pb system in the framework of the extended optical model [6–8], in which the optical potential consists of the energy independent Hartree-Fock part and the energy dependent complex polarization potential having two components, i.e., the direct reaction (DR) and fusion parts, which we call the DR and fusion potentials, respectively. In Ref. [5], using such an extended optical potential, we performed the simultaneous χ^2 analyses of the elastic scattering and fusion cross section data, determining the two components of the polarization potentials as functions of the incident energy. Our expectation was that the resulting real part of the DR potential would become repulsive consistently with the results of the CDCC calculations. Indeed the real DR polarization potential turned out to be repulsive. In addition, it was shown that both the DR and the fusion potentials satisfy the dispersion relation [9,10] separately.

In this work, we extend the analysis made in Ref. [5] to the ^{7}Li + ^{208}Pb system. In this system, such a normalization anomaly as observed in ^{6}Li + ^{208}Pb does not appear around the Coulomb barrier energies; the normalization factor N necessary for reproducing the data is close to unity, $N \approx 1$ (see Ref. [2]), in contrast to the factor $N = 0.5 \sim 0.6$ for ^{6}Li + ^{208}Pb.

In Sec. II of this article, we first discuss some characteristic features of the elastic scattering cross section data of ^{7}Li + ^{208}Pb [2] in comparison with those of ^{6}Li + ^{208}Pb. It is shown in the comparison that the DR cross section for ^{7}Li + ^{208}Pb is expected to be significantly smaller than that for ^{6}Li + ^{208}Pb. In Sec. III, we first generate the so-called semi-experimental DR cross section, $\sigma_D^{\text{semi-exp}}$, from the elastic scattering and fusion cross section data [11,12], following the method described in Ref. [13]. (Note that use is made of the fusion cross section data of ^{7}Li + ^{209}Bi, because the data are not available for ^{7}Li + ^{208}Pb.) The data of $\sigma_D^{\text{semi-exp}}$

are needed for separately determining the DR and fusion potentials. The χ^2 analyses of the elastic scattering, fusion, and semi-experimental DR cross section data are then carried out in Sec. IV. In Sec. IV, a comparison is made of the present results with those obtained from the CDCC calculations [4] and a previous study [2] based on the conventional optical model with a double folding potential. We also show a comparison of the present results with the analysis previously made by us [5] for the ^{6}Li + ^{208}Pb system. Section V concludes the paper.

II. REVIEW OF EXPERIMENTAL CROSS SECTIONS

We begin with the discussion of some of the characteristic features of the elastic scattering cross sections $d\sigma_{\rm el}/d\sigma_\Omega$ data for ^{7}Li + ^{208}Pb in comparison with those for ^{6}Li + ^{208}Pb. Such features can best be seen in the ratio P_E, defined by

$$P_E \equiv \frac{d\sigma_{\rm el}}{d\sigma_\Omega} \Big/ \frac{d\sigma_C}{d\sigma_\Omega} = d\sigma_{\rm el}/d\sigma_C, \tag{1}$$

as a function of the distance of the closest approach D (or the reduced distance d), where $d\sigma_C/d\sigma_\Omega$ is the Coulomb scattering cross section, while D (d) is related to the scattering angle θ by

$$D = d\left(A_1^{1/3} + A_2^{1/3}\right) = \frac{1}{2} D_0 \left[1 + \frac{1}{\sin(\theta/2)}\right], \tag{2}$$

with

$$D_0 = \frac{Z_1 Z_2 e^2}{E}, \tag{3}$$

D_0 being the distance of the closest approach in a head-on collision. Here (A_1, Z_1) and (A_2, Z_2) are the mass and charge of the projectile and target ions, respectively, and $E \equiv E_{\rm c.m.}$ is the incident energy in the center-of-mass system. P_E as defined by Eq. (1) is referred to as the elastic probability.

In Figs. 1(a) and 1(b), we present the experimental values of P_E for incident energies around the Coulomb barrier energy as a function of the reduced distance d for ^{7}Li + ^{208}Pb and ^{6}Li + ^{208}Pb, respectively. As seen, the values of P_E at different energies line up to form a very narrow band. This is a characteristic feature seen in many of the heavy-ion collisions, reflecting the semiclassical nature of these collisions. P_E remains close to unity until two ions approach each other within a distance d_I, where P_E begins to fall off. The distance d_I is usually called the interaction distance, at which the nuclear interactions between the colliding ions are switched on, so to speak. The values of d_I are about 1.9 fm for ^{6}Li + ^{208}Pb and 1.8 fm for ^{7}Li + ^{208}Pb.

As argued in Ref. [13], the fall off of the P_E values in the region immediately next to d_I is due to DR. The fact that the d_I value (1.9 fm) for ^{6}Li + ^{208}Pb is larger than the d_I (1.8 fm) for ^{7}Li + ^{208}Pb shows that DR starts to take place at larger distances for ^{6}Li + ^{208}Pb than it does for ^{7}Li + ^{208}Pb. Also, it can be seen that the amount of decrease of the P_E value from unity in ^{6}Li + ^{208}Pb is significantly larger than that in ^{7}Li + ^{208}Pb at 1.5 fm $< d <$ 1.9 fm, where DR takes place. These features clearly indicate that DR (which may be dominated by breakup) takes place significantly stronger in ^{6}Li + ^{208}Pb than in ^{7}Li + ^{208}Pb. This is indeed the case as can be seen in the next section from the semi-experimental DR cross section to be extracted. Finally, we note that in the region of $d < 1.5$ fm where fusion dominates, the values of P_E for ^{7}Li + ^{208}Pb and ^{6}Li + ^{208}Pb are almost identical.

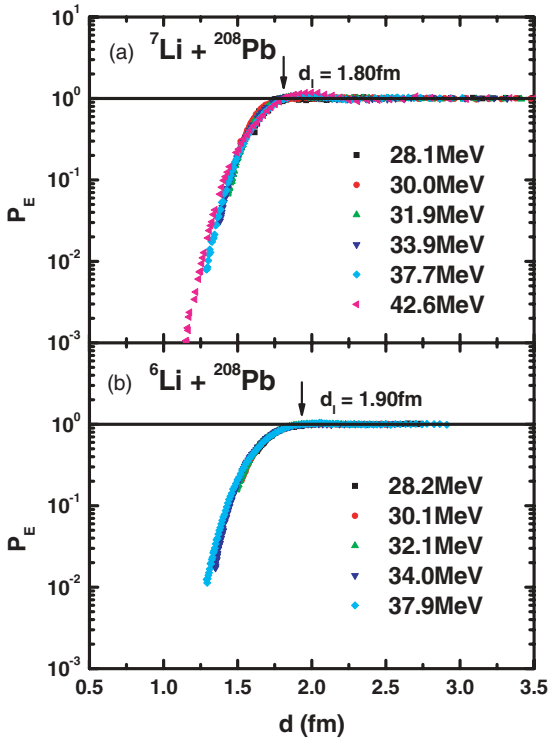

FIG. 1. (Color online) P_E values for (a) the ^{7}Li + ^{208}Pb system and (b) the ^{6}Li + ^{208}Pb system.

III. EXTRACTING SEMI-EXPERIMENTAL DR CROSS SECTION

For our purpose of determining the fusion and DR potentials separately, it is desirable to have the data of the DR cross section in addition to the data of the fusion and elastic scattering cross sections. For the ^{7}Li + ^{208}Pb system, however, no reliable data of the DR cross sections are available, although considerable efforts have been devoted to measure the breakup and incomplete fusion cross sections [11,14]. Here, we thus generate the so-called semi-experimental DR cross section $\sigma_D^{\rm semi\text{-}exp}$, following the method proposed in Ref. [13].

Our method to generate $\sigma_D^{\rm semi\text{-}exp}$ resorts to the well-known empirical fact that the total reaction cross section σ_R calculated from the optical model fit to the available elastic scattering cross section data, $d\sigma_E^{\rm exp}/d\Omega$, usually agrees well with the experimental σ_R, despite the ambiguities in the optical potential. Let us call σ_R thus generated the semi-experimental reaction cross section $\sigma_R^{\rm semi\text{-}exp}$. Then, $\sigma_D^{\rm semi\text{-}exp}$ is generated as

$$\sigma_D^{\rm semi\text{-}exp} = \sigma_R^{\rm semi\text{-}exp} - \sigma_F^{\rm exp}. \tag{4}$$

This approach seems to work even for loosely bound projectiles, as demonstrated by Kolata *et al.* [15] for the ^{6}He + ^{209}Bi

system. As already noted in Sec. I, $\sigma_F^{\rm exp}$ data are not available for ^{7}Li + ^{208}Pb, and thus we use the $\sigma_F^{\rm exp}$ data taken for ^{7}Li + ^{209}Bi [11,12].

Following Ref. [13], we first carry out rather simple optical model χ^2 analyses of elastic scattering data solely for the purpose of deducing σ_R and $\sigma_R^{\rm semi\text{-}exp}$. For these preliminary analyses, we assume the optical potential to be the sum of $V_0(r) + iW_I(r)$ and $U_1(r, E)$, where $V_0(r)$ is the real, energy independent bare folding potential discussed later in Sec. IV B, $iW_I(r)$ is an energy independent short range imaginary potential discussed in Sec. IV A, and $U_1(r, E)$ is a Woods-Saxon type complex potential with common geometrical parameters for both real and imaginary parts. The elastic scattering data are then fitted with a fixed radius parameter r_1 for $U_1(r, E)$, treating, however, all three other parameters, the real and the imaginary strengths V_1 and W_1 and the diffuseness parameter a_1, as adjustable. The χ^2 fitting is done for three choices of the radius parameter: $r_1 = 1.3$, 1.4, and 1.5 fm. These different choices of the r_1 value are made to examine the dependence of the resulting $\sigma_R^{\rm semi\text{-}exp}$ on the value of r_1.

As observed in Ref. [13], the values of $\sigma_R^{\rm semi\text{-}exp}$ thus extracted for three different r_1 values agree with the average value of $\sigma_R^{\rm semi\text{-}exp}$ within 2%, implying that $\sigma_R^{\rm semi\text{-}exp}$ is determined without much ambiguity. We then identified the average values as the final values of $\sigma_R^{\rm semi\text{-}exp}$ at each energy. Using thus determined $\sigma_R^{\rm semi\text{-}exp}$, we generated $\sigma_D^{\rm semi\text{-}exp}$ by employing Eq. (4). The resultant values of $\sigma_R^{\rm semi\text{-}exp}$ and $\sigma_D^{\rm semi\text{-}exp}$ are presented in Table I, together with $\sigma_F^{\rm exp}$. In Table I, the $\sigma_R^{\rm semi\text{-}exp}$ determined in Ref. [2] are also given. It is noticeable that the two sets of $\sigma_R^{\rm semi\text{-}exp}$ determined independently agree within 1%. We can also see that the values of $\sigma_D^{\rm semi\text{-}exp}$ thus deduced are smaller than those for ^{6}Li + ^{208}Pb [5] by a factor of 1.23 $\sim$ 1.72 as anticipated from the P_E values discussed in the previous section.

IV. SIMULTANEOUS χ^2 ANALYSES

Simultaneous χ^2 analyses were then performed on the data sets of $(d\sigma_E^{\rm exp}/d\Omega, \sigma_D^{\rm semi\text{-}exp}, \sigma_F^{\rm exp})$, by taking the data for $d\sigma_E^{\rm exp}/d\Omega$ and $\sigma_F^{\rm exp}$ from the literature [2,11,12]. In calculating the χ^2 value, we simply assume 1% errors for all the experimental data. The 1% error is about the average of errors in the measured elastic scattering cross sections, but is much smaller than the errors in the DR ($\sim$5%) and fusion ($\sim$10%) cross sections. Assigning the 1% error for the DR and fusion cross sections is thus equivalent to increasing the weight for the DR and fusion cross sections in evaluating the χ^2 values by factors of 25 and 100, respectively. Such a choice of errors may be reasonable, because we have only one datum point for each of these cross sections, while there are more than 50 data points for the elastic scattering cross sections.

TABLE I. Semi-experimental total reaction and DR cross sections for the ^{7}Li + ^{208}Pb system.

$E_{\rm lab}$ (MeV)	E (MeV)	$\sigma_F^{\rm exp}$ [11,12] (mb)	$\sigma_D^{\rm semi\text{-}exp}$ (mb)	$\sigma_R^{\rm semi\text{-}exp}$ (mb)	$\sigma_R^{\rm semi\text{-}exp}$ [2] (mb)
29	28.1	18	119	137	138
31	30.0	88	240	328	327
33	31.9	218	351	569	572
35	33.9	366	418	784	787
39	37.7	650	583	1233	1242
44	42.6	866	684	1550	1553

A. Necessary formulas

The optical potential $U(r, E)$ we use in the present work has the following form:

$$U(r; E) = V_C(r) - [V_0(r) + U_F(r; E) + U_D(r; E)], \quad (5)$$

where $V_C(r)$ is the usual Coulomb potential with $r_C = 1.25$ fm and $V_0(r)$ is the bare nuclear potential, for which use is made of the double folding potential described in the next subsection. $U_F(r; E)$ and $U_D(r; E)$ are, respectively, the fusion and DR parts of the so-called polarization potential [16] that originates from couplings to the respective reaction channels. Both $U_F(r; E)$ and $U_D(r; E)$ are complex and their forms are assumed to be of volume type and surface-derivative type [7,17], respectively. $U_F(r; E)$ and $U_D(r; E)$ are explicitly given by

$$U_F(r; E) = [V_F(E) + iW_F(E)]f(X_F) + iW_I(r), \quad (6)$$

and

$$U_D(r; E) = [V_D(E) + iW_D(E)]4a_D\frac{df(X_D)}{dR_D}, \quad (7)$$

where $f(X_i) = [1 + \exp(X_i)]^{-1}$ with $X_i = (r - R_i)/a_i$ ($i = F$ and D) is the usual Woods-Saxon function with the fixed geometrical parameters of $r_F = 1.40$ fm, $a_F = 0.33$ fm, $r_D = 1.47$ fm, and $a_D = 0.56$ fm, while $V_F(E)$, $V_D(E)$, $W_F(E)$, and $W_D(E)$ are the energy dependent strength parameters. Because we assume the geometrical parameters to be the same for both the real and the imaginary potentials, the strength parameters $V_i(E)$ and $W_i(E)$ ($i = F$ or D) are related through a dispersion relation [9],

$$V_i(E) = V_i(E_s) + \frac{E - E_s}{\pi}{\rm P}\int_0^\infty dE'\frac{W_i(E')}{(E' - E_s)(E' - E)}, \quad (8)$$

where P stands for the principal value and $V_i(E_s)$ is the value of $V_i(E)$ at a reference energy $E = E_s$. Later, we will use Eq. (8) to generate the final real strength parameters $V_F(E)$ and $V_D(E)$ using $W_F(E)$ and $W_D(E)$ fixed from the χ^2 analyses. Note that the breakup cross section may include contributions from both Coulomb and nuclear interactions, which implies that the direct reaction potential includes effects coming from not only the nuclear interaction but also from the Coulomb interaction.

The last imaginary potential $W_I(r)$ in $U_F(r; E)$ given by Eq. (6) is a short range potential of the Woods-Saxon type given as

$$W_I(r) = W_I f(X_I), \quad (9)$$

with $W_I = 40$ MeV, $r_I = 0.8$ fm, and $a_I = 0.30$ fm. This imaginary potential was first introduced [5] to eliminate

unphysical reflection in the radial wave functions of low partial waves when this $W_I(r)$ is absent. Because of the large strength of the folding potential V_0 used in this study and also because $W_F(E)f(X_F)$ of Eq. (6) turns out to be not strong enough, reflections of lower partial waves appear in the asymptotic region, which causes unphysical oscillations of differential elastic cross sections at large angles, particularly at relatively high energies above the Coulomb barrier, but physically such reflection should not occur because of the strong absorption that should exist inside the nucleus. $W_I(r)$ is thus introduced to take care of the strong absorption inside and eliminate this unphysical effect. We might then need to introduce a real part $V_I(r)$ corresponding to $W_I(r)$, but we ignored the real part, simply because such a real potential did not affect at all the real physical observables, which means that it is impossible to extract the information on $V_I(r)$ from the analyses of the experimental data. Further, as is discussed later in Sec. IV.E, $W_I(r)$ is also insensitive to the observables, particularly at low energies around and below the Coulomb barrier. This means that it is also impossible to extract information of the energy dependence of $W_I(r)$ from the data. For this reason, we simply ignore in this study the energy dependence of $W_I(r)$.

In the extended optical model, fusion and DR cross sections, $\sigma_F^{\rm th}$ and $\sigma_D^{\rm th}$, respectively, are calculated by using the expression [6–8,18]

$$\sigma_i^{\rm th} = \frac{2}{\hbar v}\langle\chi^{(+)}|{\rm Im}[U_i(r;E)]|\chi^{(+)}\rangle \qquad (i = F \text{ or } D), \quad (10)$$

where $\chi^{(+)}$ is the usual distorted wave function that satisfies the Schrödinger equation with the full optical model potential $U(r;E)$ in Eq. (5). $\sigma_F^{\rm th}$ and $\sigma_D^{\rm th}$ are thus calculated within the same framework as $d\sigma_{el}/d\Omega$ is calculated. Such a unified description enables us to evaluate all the different types of cross sections on the same footing.

B. The folding potential

The double folding potential $V_0(r)$ we use in the present study as the bare potential may be written as [1]

$$V_0(r) = \int d\mathbf{r}_1 \int d\mathbf{r}_2 \rho_1(r_1)\rho_2(r_2)v_{NN}(r_{12} = |\mathbf{r} - \mathbf{r}_1 + \mathbf{r}_2|), \quad (11)$$

where $\rho_1(r_1)$ and $\rho_2(r_2)$ are the nuclear matter distributions for the target and projectile nuclei, respectively, while v_{NN} is the sum of the M3Y interaction that describes the effective nucleon-nucleon interaction and the knockon exchange effect given as

$$v_{NN}(r) = 7999\frac{e^{-4r}}{4r} - 2134\frac{e^{-2.5r}}{2.5r} - 262\delta(r). \quad (12)$$

We use for $\rho_1(r)$ the following Woods-Saxon form taken from Ref. [19],

$$\rho_1(r) = \rho_0 / \left[1 + \exp\left(\frac{r-c}{z}\right)\right], \quad (13)$$

with $c = 6.624$ fm and $z = 0.549$ fm, while for $\rho_2(r)$ the following is taken from Ref. [20],

$$\rho_2(r) = (A + Br^2)e^{-\alpha^2 r^2}, \quad (14)$$

with $A = 0.13865$ fm^{-3}, $B = 0.02316$ fm^{-1}, and $\alpha = 0.578$ fm^{-1}. We then use the code DFPOT of Cook [21] for evaluating $V_0(r)$.

C. Threshold energies of subbarrier fusion and DR

As in Ref. [5], we utilize as an important ingredient the so-called threshold energies $E_{0,F}$ and $E_{0,D}$ of subbarrier fusion and DR, respectively, which are defined as zero intercepts of the linear representation of the quantities $S_i(E)$, defined by

$$S_i \equiv \sqrt{E\sigma_i} \approx \alpha_i(E - E_{0,i}) \, (i = F \text{ or } D), \quad (15)$$

where α_i is a constant. S_i with $i = F$, i.e., S_F, is the quantity introduced originally by Stelson *et al.* [22], who showed that in the subbarrier region S_F from the measured σ_F can be represented very well by a linear function of E (linear systematics) as in Eq. (15). In Ref. [17], we extended the linear systematics to DR cross sections. In fact the DR data are also well represented by a linear function.

In Fig. 2, we present the experimental $S_F(E)$ and $S_D(E)$. For $S_D(E)$, use is made of $\sigma_D^{\rm semi\text{-}exp}$. From the zeros of $S_i(E)$, one can deduce $E_{0,D}^{\rm semi\text{-}exp} = 19.3$ MeV and $E_{0,F}^{\rm exp} = 26.5$ MeV. For both $i = F$ and D, the observed S_i are very well approximated by straight lines in the subbarrier region and thus $E_{0,i}$ can be extracted without much ambiguity. It is worthwhile to remark that $E_{0,D}^{\rm semi\text{-}exp}$ is found to be considerably smaller than $E_{0,F}^{\rm exp}$, implying that DR channels open at smaller energies than fusion channels, which seems physically reasonable.

$E_{0,i}$ may then be used as the energy where the imaginary potential $W_i(E)$ becomes zero, i.e., $W_i(E_{0,i}) = 0$ [17,23]. This procedure is used later in the next subsection for obtaining a mathematical expression for $W_i(E)$.

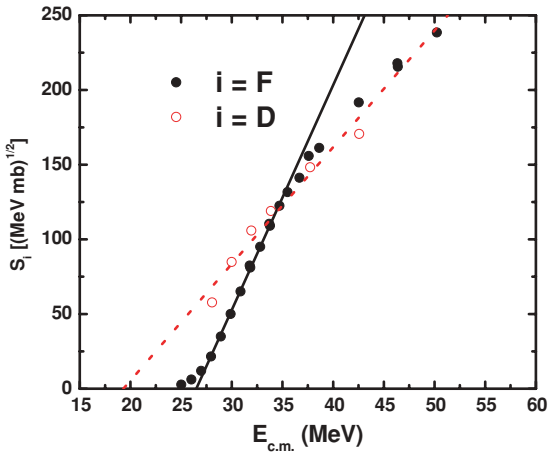

FIG. 2. (Color online) The Stelson plot of $S_i = \sqrt{E\sigma_i}$ for DR ($i = D$, open circles) and fusion ($i = F$, filled circles) cross sections. Use is made of the semi-experimental DR cross section for S_D, while the experimental fusion cross section is employed for S_F. The intercepts of the straight lines with the energy axis give us the threshold energies $E_{0,D}^{\rm semi\text{-}exp} = 19.3$ MeV and $E_{0,F}^{\rm exp} = 26.5$ MeV.

D. χ^2 analyses

All the χ^2 analyses performed in the present work are carried out by using the folding potential as its bare potential $V_0(r)$ described in Sec. IV B and by using the fixed geometrical parameters for the polarization potentials, $r_F = 1.40$ fm, $a_F = 0.33$ fm, $r_D = 1.47$ fm, and $a_D = 0.56$ fm, which are close to the values used in our previous study [17]. A slight change of the values used in Ref. [17] is made to improve the χ^2 fitting.

As in Ref. [17], the χ^2 analyses are done in two steps; in the first step, all four strength parameters, $V_F(E)$, $W_F(E)$, $V_D(E)$ and $W_D(E)$, are varied. In this step, we could fix fairly well the strength parameters of the DR potential, $V_D(E)$ and $W_D(E)$, in the sense that $V_D(E)$ and $W_D(E)$ were determined as a smooth function of E. The values of $V_D(E)$ and $W_D(E)$ thus extracted are presented in Fig. 3 by open circles. The values of $W_D(E)$ can be well represented by the following function of E (in units of MeV)

$$W_D(E) = \begin{cases} 0 & \text{for } E \leqslant E_{0,D}^{\text{semi-exp}} = 19.3 \\ 0.075(E - 19.3) & \text{for } 19.3 < E \leqslant 29.3 \\ 0.75 & \text{for } 29.3 < E. \end{cases} \tag{16}$$

Note that the threshold energy where $W_D(E)$ becomes zero is set equal to $E_{0,D}^{\text{semi-exp}}$ as determined in the previous subsection and is indicated by the open circle at $E = 19.3$ MeV in Fig. 3. The dotted line in the lower panel of Fig. 3 represents Eq. (16), while that in the upper panel of Fig. 3 denotes V_D as calculated by the dispersion relation Eq. (8), with $W_D(E)$ given by Eq. (16). As seen, the dotted lines reproduce the open circles quite well, indicating that $V_D(E)$ and $W_D(E)$ extracted by the χ^2 analyses satisfy the dispersion relation.

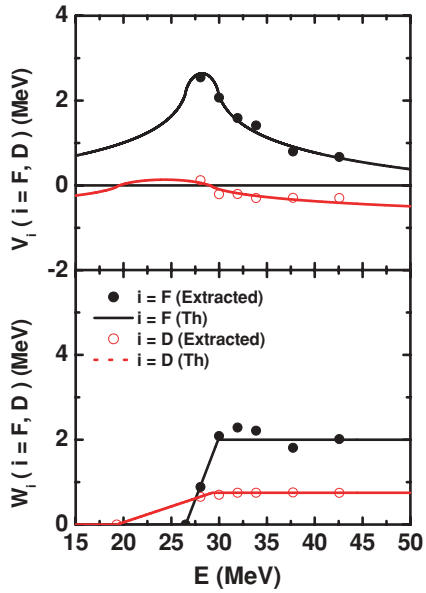

FIG. 3. (Color online) The strength parameters V_i (upper panel) and W_i (lower panel) for $i = D$ and F as functions of $E_{\text{c.m.}}$. The open and filled circles are the strength parameters for $i = D$ and F, respectively. The dotted and solid lines in the lower panel denote W_D and W_F from Eqs. (16) and (17), respectively, while the dotted and solid curves in the upper panel represent V_D and V_F calculated by using the dispersion relation of Eq. (8) with W_i given by Eqs. (16) and (17). The potential values and the corresponding reference energies used in Eq. (8) are such that V_F ($E_s = 29.9$ MeV) $= 2.2$ MeV and V_D ($E_s = 29.3$ MeV) $= -0.03$ MeV, respectively.

In this first step of χ^2 fitting, however, the values of $V_F(E)$ and $W_F(E)$ are not reliably fixed in the sense that the extracted values fluctuate considerably as functions of E. This is understandable from the expectation that the elastic scattering data can probe most accurately the optical potential in the peripheral region, which is nothing but the region characterized by the DR potential. The part of the nuclear potential responsible for fusion is thus difficult to pin down in this first step.

To obtain more reliable information on V_F and W_F, we thus performed the second step of the χ^2 analysis; this time, instead of doing a four-parameter search, we fixed V_D and W_D as determined by the first χ^2 fitting, i.e., $W_D(E)$ given by Eq. (16) and $V_D(E)$ predicted from the dispersion relation. We then performed two-parameter χ^2 analyses, treating only $V_F(E)$ and $W_F(E)$ as adjustable parameters. The values thus determined are presented in Fig. 3 by filled circles. As seen, both $V_F(E)$ and $W_F(E)$ are determined to be fairly smooth functions of E. The $W_F(E)$ values may be represented by

$$W_F(E) = \begin{cases} 0 & \text{for } E \leqslant E_{0,F}^{\text{exp}} = 26.5 \\ 0.588(E - 26.5) & \text{for } 26.5 < E \leqslant 29.9 \\ 2.00 & \text{for } 29.9 < E. \end{cases} \tag{17}$$

As is done for $W_D(E)$, the threshold energy where $W_F(E)$ becomes zero is set equal to $E_{0,F}^{\text{exp}}$, which is also indicated by the filled circles in Fig. 3. As seen, the $W_F(E)$ values determined by the second χ^2 analyses can fairly well be represented by the functions given by Eq. (17). Note that the energy variations seen in $W_F(E)$ and $V_F(E)$ are more rapid compared with those seen in $W_D(E)$ and $V_D(E)$ and are similar to those observed with tightly bound projectiles [24–26]. It is thus seen that the resultant $V_F(E)$ and $W_F(E)$ exhibit the threshold anomaly.

Using $W_F(E)$ given by Eq. (17), one can generate $V_F(E)$ from the dispersion relation. The results are shown by the solid curve in the upper panel of Fig. 3, which again well reproduces the values extracted from the χ^2 fitting. This means that the fusion potential determined from the present analysis also satisfies the dispersion relation.

E. Final calculated cross sections in comparison with the data

Using $W_D(E)$ given by Eq. (16) and $W_F(E)$ given by Eq. (17) together with $V_D(E)$ and $V_F(E)$ generated by the dispersion relation, we performed the final calculations of the elastic, DR, and fusion cross sections. The results are presented in Figs. 4 and 5 in comparison with the experimental data. All the data are well reproduced by the calculations.

It may be worth noting here that the theoretical fusion cross section, σ_F^{th}, includes contributions from two imaginary components, $W_I(r)$ and $W_F(E) f(X_F)$ in $U_F(r, E)$ of Eq. (6). In Table II the partial contributions from the $W_I(r)$ part, denoted by σ_I, are presented in comparison with the total calculated fusion cross section, σ_F^{th}. As seen, the contribution from the inner part, W_I, amounts to $22 \sim 46\%$ of σ_F^{th}, which is relatively small but not negligible at all.

TABLE II. Partial contributions σ_I and σ_F to the fusion cross sections.

$E_{\rm lab}$ (MeV)	E (MeV)	σ_I (mb)	σ_F (mb)	$\sigma_F^{\rm th}$ (mb)
29	28.1	11	13	24
31	30.0	23	80	103
33	31.9	53	166	219
35	33.9	91	259	350
39	37.7	175	430	605
44	42.6	277	604	881

Despite this non-negligible contribution from $W_I(r)$, $W_I(r)$ is rather insensitive to the final total fusion cross section, $\sigma_F^{\rm th}$, and also to the elastic scattering cross sections, particularly in the energy region where the strength of $W_F(E)$ varies rapidly with E. To see this, we repeated the cross section calculations by reducing the value of W_I to 20 MeV at $E = 28.1$ MeV. This energy is the lowest energy considered in the present study and is a typical energy in the region where $W_F(E)$ changes rapidly with E. The resulting elastic scattering cross section is found to remain essentially the same. The value of σ_I decreases from 11 to 10 mb, and σ_F increases from 13 to 14 mb, leaving the total fusion cross section, $\sigma_F^{\rm th}$, unchanged. This result confirms what was stated earlier in Sec. IV A, that it is impossible to extract information of the energy dependence of W_I from the analysis of the experimental data, justifying the present approach to treat W_I as a constant.

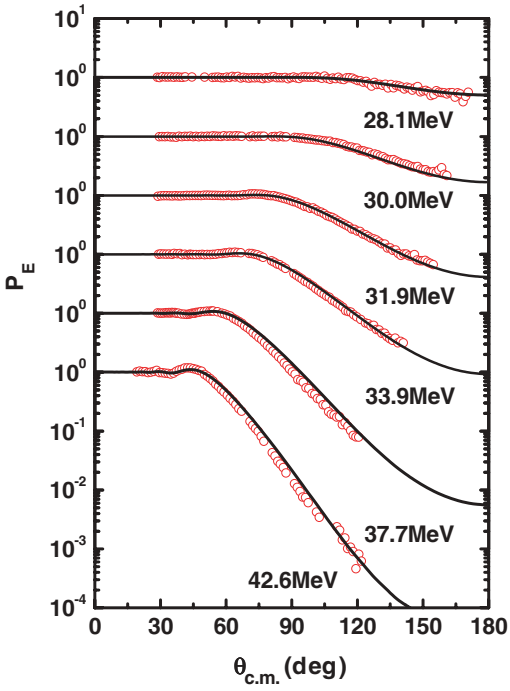

FIG. 4. (Color online) Ratios of the elastic scattering cross sections to the Rutherford cross section calculated with our final dispersive optical potential are shown in comparison with the experimental data. The data are taken from Ref. [2].

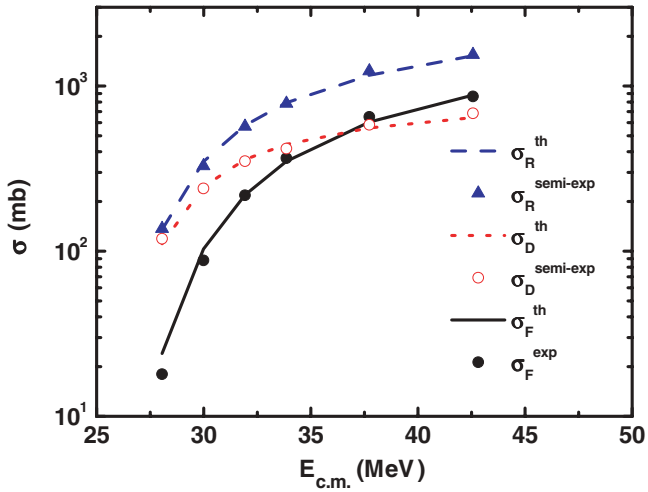

FIG. 5. (Color online) DR and fusion cross sections calculated with our final dispersive optical potentials are shown in comparison with the experimental data. $\sigma_D^{\rm semi\text{-}exp}$ denoted by the open circles are obtained as described in Sec. II. The fusion data are from Refs. [11] and [12].

F. Discussions

As already noted in Sec. IV D, the real and imaginary parts of both DR and fusion polarization potentials determined from the present χ^2 analyses satisfy the dispersion relation [9,10] separately. Furthermore, the fusion potential exhibits the threshold anomaly as observed in heavy-ion collisions involving tightly bound projectiles [24–26]. For the ^{6}Li + ^{208}Pb system studied earlier [5] similar threshold anomalies for the fusion potential and the dispersion relation were observed.

It is remarkable that the real part of the DR potential, which we denote here by $V_D(r, E)$, turns out to be repulsive at most of the energies considered; only exceptions appear at the lowest energy point of $E = 28.1$ MeV, where $V_D(r, E)$ becomes very weakly attractive (see Fig. 3). The final dispersive $V_D(r, E)$ determined by using the dispersion relation, Eq. (8), with $W_D(E)$ given by Eq. (16) is repulsive above $E \simeq 29$ MeV, but becomes weakly attractive between $E = 19$ and 29 MeV. We remark that the repulsiveness of $V_D(r, E)$ for ^{7}Li + ^{208}Pb is considerably weaker than that for ^{6}Li + ^{208}Pb [5], which is consistent with the results drawn from the CDCC study made in Ref. [4], where the polarization potentials due to the coupling to the breakup channels are calculated for both ^{6}Li + ^{208}Pb and ^{7}Li + ^{208}Pb.

It is also remarkable that the polarization potential in the surface region, say at the strong absorption radius of $R_{\rm sa} = 12.4$ fm, is dominated by the DR part of the potential as shown in Fig. 6. (Note that Fig. 3 shows only the potential strength parameters, not the potential values.) The same is true for ^{6}Li + ^{208}Pb in Ref. [5]. Let us take as an example the imaginary part of the potential. Then the contribution to the total imaginary part of the potential from the fusion part is less than 6 and 15% for ^{7}Li + ^{208}Pb and ^{6}Li + ^{208}Pb systems, respectively. Therefore, the total polarization potential in the surface region is mainly characterized by the DR potential.

It is then interesting to compare the values of the total imaginary potential at $r = R_{\rm sa}$, $W(r = R_{\rm sa}, E)$, with those

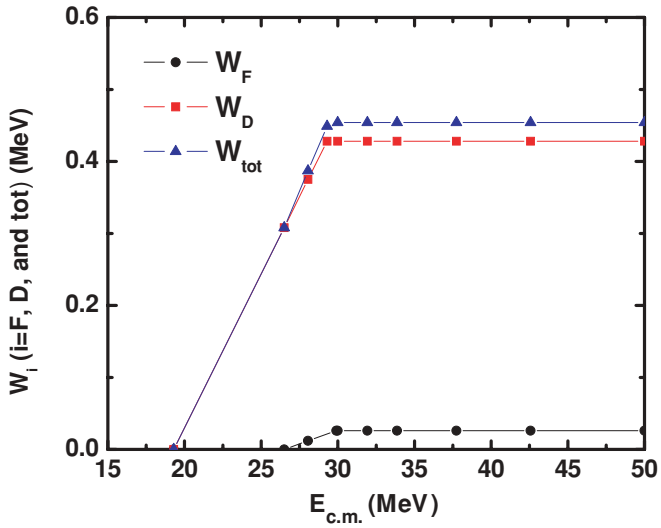

FIG. 6. (Color online) The values of $W_F(r, E)$, $W_D(r, E)$, and the sum $W_{\rm tot}(r, E) = W_F(r, E) + W_D(r, E)$ as functions of E calculated by using Eqs. (6), (7), (16), and (17) at the strong absorption radius, $r = R_{\rm sa} = 12.4$ fm, for all energies.

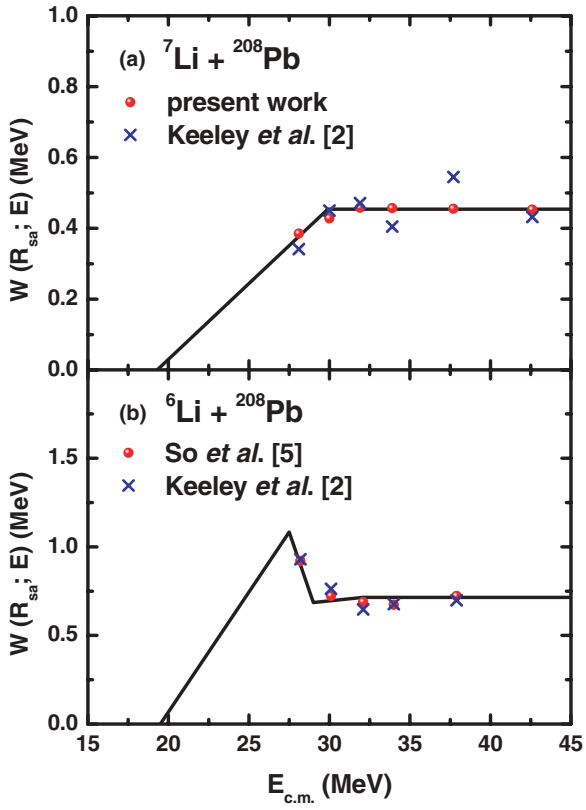

FIG. 7. (Color online) The values of the total imaginary potential $W(r, E)$ at $r = R_{\rm sa} = 12.4$ fm deduced in the present χ^2 analyses and those obtained in Ref. [2]. The values from Ref. [2] are multiplied by factors 1.23 and 1.11 for the ^{7}Li + ^{208}Pb and ^{6}Li + ^{208}Pb systems, respectively.

obtained in Ref. [2], where the χ^2 analyses of the elastic scattering data of both ^{6}Li + ^{208}Pb and ^{7}Li + ^{208}Pb were carried out by using double folding potentials as a real potential and a Woods-Saxon type as an imaginary potential. In Ref. [2] the overall normalization constant N of the double folding potential and all three parameters (the strength, radius, and diffuseness parameters) of the imaginary potential were treated as adjustable parameters. An important conclusion drawn from the analyses was that the resultant potentials at the surface exhibit the threshold anomaly for ^{7}Li but not for ^{6}Li.

In Fig. 7, presented are values of $W(r, E)$, at $r = R_{\rm sa} = 12.4$ fm, obtained directly from the χ^2 analyses [not those of the dispersive potential such as given by Eqs. (16) and (17)] carried out here for ^{7}Li and in Ref. [5] for ^{6}Li in comparison with those taken from Fig. 2 of Ref. [2]. Note that the potential values taken from Ref. [2] are multiplied by factors 1.23 and 1.11 for ^{7}Li and ^{6}Li, respectively, for comparison. Figure 7 shows that the two sets of the values are very close to each other, demonstrating clearly that the energy dependencies of the $W(R_{\rm sa}, E)$ values determined in both cases are essentially the same. Combined with the above-mentioned fact that the $W(R_{\rm sa}, E)$ values determined in the present study and in Ref. [5] are essentially those of the DR potential, it follows that the energy dependence seen in the $W(R_{\rm sa}, E)$ values of Ref. [2] is that of DR. In this sense, the threshold anomaly claimed to be seen in Ref. [2] for ^{7}Li is not the threshold anomaly due to fusion that was copiously observed in the tightly bound projectiles [24–26].

V. CONCLUSIONS

Simultaneous χ^2 analyses are made for elastic scattering and fusion cross section data for the ^{7}Li + ^{208}Pb system at near-Coulomb-barrier energies based on the extended optical model approach in which the polarization potential is decomposed into DR and fusion parts. Use is made of the double folding potential as a bare potential. It is found that the experimental elastic scattering and fusion data are well reproduced without introducing any normalization factor for the double folding potential and also that both DR and fusion parts of the polarization potential determined from the χ^2 analyses satisfy separately the dispersion relation. Moreover, we find that the real part of the fusion portion of the polarization potential is attractive while that of the DR part is repulsive except at energies far below the Coulomb barrier energy. The repulsive real part of the DR potential is, however, considerably smaller than that for ^{6}Li + ^{208}Pb obtained earlier [5], reflecting the fact that the DR (breakup) cross section for ^{7}Li + ^{208}Pb is smaller than that for ^{6}Li + ^{208}Pb. Accordingly, the imaginary part of the DR potential obtained for ^{7}Li + ^{208}Pb is smaller than that for ^{6}Li + ^{208}Pb. These features of the polarization potential remarked above are qualitatively consistent with those obtained in the CDCC calculation [2].

We find that the energy dependence of the optical potential determined in Ref. [2] is very much like that of the DR potential deduced in the present study.This means that the energy dependence seen in Ref. [2] is not a real threshold anomaly due to fusion, but rather is a much more slowly varying energy dependence due to DR.

ACKNOWLEDGMENTS

This work was supported in part by Korea Research Foundation grants funded by the Korean Government (MOEHRD) (KRF-2006-214-C00014 and KRF-2003-070-C00015). It was also supported in part by a Korea Science and Engineering Foundation grant funded by the Korean Government (MOST) (M20608520001-06B0852-00110).

[1] G. R. Satchler and W. G. Love, Phys. Rep. **55**, 183 (1979).
[2] N. Keeley, S. J. Bennett, N. M. Clarke, B. R. Fulton, G. Tungate, P. V. Drumm, M. A. Nagarajan, and J. S. Lilly, Nucl. Phys. **A571**, 326 (1994).
[3] Y. Sakuragi, Phys. Rev. C **35**, 2161 (1987).
[4] N. Keeley and K. Rusek, Phys. Lett. **B427**, 1 (1998).
[5] W. Y. So, T. Udagawa, K. S. Kim, S. W. Hong, and B. T. Kim, Phys. Rev. C **75**, 024610 (2007).
[6] T. Udagawa, B. T. Kim, and T. Tamura, Phys. Rev. C **32**, 124 (1985); T. Udagawa and T. Tamura, *ibid.* **29**, 1922 (1984).
[7] S.-W. Hong, T. Udagawa, and T. Tamura, Nucl. Phys. **A491**, 492 (1989).
[8] T. Udagawa, T. Tamura, and B. T. Kim, Phys. Rev. C **39**, 1840 (1989); B. T. Kim, M. Naito, and T. Udagawa, Phys. Lett. **B237**, 19 (1990).
[9] C. Mahaux, H. Ngõ, and G. R. Satchler, Nucl. Phys. **A449**, 354 (1986); **A456**, 134 (1986).
[10] M. A. Nagarajan, C. C. Mahaux, and G. R. Satchler, Phys. Rev. Lett. **54**, 1136 (1985).
[11] M. Dasgupta, P. R. S. Gomes, D. J. Hinde, S. B. Moraes, R. M. Anjos, A. C. Berriman, R. D. Butt, N. Carlin, J. Lubian, C. R. Morton, J. O. Newton, and A. Szanto de Toledo, Phys. Rev. C **70**, 024606 (2004).
[12] M. Dasgupta, D. J. Hinde, K. Hagino, S. B. Moraes, P. R. S. Gomes, R. M. Anjos, R. D. Butt, A. C. Berriman, N. Carlin, C. R. Morton, J. O. Newton, and A. Szanto de Toledo, Phys. Rev. C **66**, 041602(R) (2002).
[13] W. Y. So, S. W. Hong, B. T. Kim, and T. Udagawa, Phys. Rev. C **69**, 064606 (2004).
[14] C. Signorini, M. Mazzocco, G. F. Prete, F. Soramel, L. Stroe, A. Andrighetto, I. J. Thompson, A. Vitturi, A. Brondi, M. Cinausero, D. Fabris, E. Fioretto, N. Gelli, J. Y. Guo, G. La Rana, Z. H. Liu, F. Lucarelli, R. Moro, G. Nebbia, M. Trotta, E. Vardaci, and G. Viesti, Eur. Phys. J. A **10**, 249 (2001).
[15] J. J. Kolata, V. Guimarães, D. Peterson, P. Santi, R. White-Stevens, P. A. DeYoung, G. F. Peaslee, B. Hughey, B. Atalla, M. Kern, P. L. Jolivette, J. A. Zimmerman, M. Y. Lee, F. D. Becchetti, E. F. Aguilera, E. Martinez-Quiroz, and J. D. Hinnefeld, Phys. Rev. Lett. **81**, 4580 (1998).
[16] W. G. Love, T. Terasawa, and G. R. Satchler, Nucl. Phys. **A291**, 183 (1977).
[17] B. T. Kim, W. Y. So, S. W. Hong, and T. Udagawa, Phys. Rev. C **65**, 044607 (2002).
[18] M. S. Hussein, Phys. Rev. C **30**, 1962 (1984).
[19] C. W. De Jager, H. DeVries, and C. DeVries, At. Data Nucl. Data Tables **14**, 479 (1974).
[20] J. Cook, M. F. Vineyard, K. W. Kemper, and V. Hnizdo, Phys. Rev. C **27**, 1536 (1983).
[21] J. Cook, Comput. Phys. Commun. **25**, 125 (1982).
[22] P. H. Stelson, Phys. Lett. **B205**, 190 (1988); P. H. Stelson, H. J. Kim, M. Beckerman, D. Shapira, and R. L. Robinson, Phys. Rev. C **41**, 1584 (1990).
[23] B. T. Kim, W. Y. So, S. W. Hong, and T. Udagawa, Phys. Rev. C **65**, 044616 (2002).
[24] A. Baeza, B. Bilwes, R. Bilwes, J. Diaz, and J. L. Ferrero, Nucl. Phys. **A419**, 412 (1984).
[25] J. S. Lilley, B. R. Fulton, M. A. Nagarajan, I. J. Thompson, and D. W. Banes, Phys. Lett. **B151**, 181 (1985).
[26] B. R. Fulton, D. W. Banes, J. S. Lilley, M. A. Nagarajan, and I. J. Thompson, Phys. Lett. **B162**, 55 (1985).